AIAA JOURNAL
Vol. 50, No. 12, December 2012

Disturbance Level Characterization of a Hypersonic Blowdown Facility

Davide Masutti,* Emanuele Spinosa,† Olivier Chazot,‡ and Mario Carbonaro§
von Kármán Institute for Fluid Dynamics, 1640 Rhode-St-Genèse, Belgium

DOI: 10.2514/1.J051502

Freestream disturbance levels were measured in the Mach 6 Hypersonic Wind Tunnel H3 of the von Kármán Institute, for unit Reynolds numbers ranging from 9.9×10^6 to 27.3×10^6 m^{-1}. A detailed characterization was performed using a dual hot-wire anemometer probe operated in the constant temperature mode and a fast response pressure transducer mounted on the tip of a pitot probe. The disturbance levels measured by the two instruments indicated normalized fluctuating values of 5.2, 0.8, and 1.7%, respectively, for mass flux, total temperature, and pitot pressure. Statistical and spectral analyses were compared with data available in the literature and agreed with values obtained for other hypersonic wind tunnels working at similar ranges of Mach and Reynolds numbers. A combined data reduction technique allowed a complete analysis of the freestream flow. Normalized fluctuations of velocity, static temperature, and density were found to be 0.6, 5.2, and 4.9% respectively. Moreover, the dominant role of the sound-wave mode was observed in agreement with the features of conventional noisy hypersonic wind tunnels.

Nomenclature

C_P	=	pressure coefficient
C_p	=	specific heat at constant pressure
M	=	Mach number
p	=	pressure, Pa
p_t	=	pitot pressure
Re	=	Reynolds number, 1/m
T	=	temperature, K
U	=	velocity, m/s
Θ	=	entropy mode
ρ	=	density, kg/m^3
σ	=	sound-wave mode
ω	=	vorticity mode

Subscripts

0	=	stagnation quantity
∞	=	freestream quantity

Accents

$'$	=	instantaneous value
$\bar{}$	=	time-averaged value

I. Introduction

THE assessment of the flow quality of a wind tunnel dedicated to ground testing is a key issue, especially in transition studies. It is well known that freestream disturbances and flow quantity fluctuations have a dominant role on boundary-layer stability, especially at high speeds. In Fig. 1, a schematic of the different mechanisms leading to boundary-layer transition, according to Morkovin et al. [1] is presented. Different paths to boundary-layer transition exist according to the intensity of the initial disturbance level: Some parts of the process may be bypassed or may not exist at all. The coupling between model shear layer and freestream flow disturbances is referred to in the literature as the receptivity problem and is still largely unsolved. A brief review of boundary-layer receptivity issues and their relation to freestream disturbances is provided by Saric et al. [2] and Pate [3]. The level of disturbances, in a more practical reasoning, also affects the location of the natural boundary-layer transition on a vehicle surface. In flight conditions, the noise level of the flow is usually very low compared with the wind-tunnel environment: this leads to a discrepancy between the location of the transition region in ground testing and in flight. Therefore, a knowledge of the disturbance level of the wind-tunnel facility is important both to build transition models and to extrapolate ground test results to flight conditions [4].

It is not only important to quantitatively assess the intensity of the disturbances, but also to characterize their nature and origin. To outline the main characteristics of a compressible turbulent flowfield (such as the freestream flow in supersonic or hypersonic wind tunnels) by means of analytical methods, Kovasznay [5] developed a simplified analysis. According to this small perturbation analysis, the fluctuations of a gas moving at a supersonic speed can be considered at any point as a superposition of three modes of covarying physical properties: a sound-wave mode (variation of pressure, density, and temperature as well as that of the coupled irrotational field at constant entropy), also referred to as the acoustic mode; an entropy mode (variation of entropy, density, and temperature at constant pressure, also mentioned as entropy spottiness or temperature spottiness mode); and a vorticity mode (variation of the solenoidal component of the velocity field, which is known as simple "turbulence" at low speeds). In the case of a freestream flow in a supersonic/hypersonic wind tunnel, the entropy and vorticity modes are convected essentially along streamlines and may be related to the conditions of the settling chamber, whereas sound-wave disturbances travel across the streamlines and may arise from the settling chamber, the test section, and the nozzle. Morkovin [6] provided a further classification of sound-wave mode disturbances, also reported in Schneider [7], separating them in eddy Mach waves and shivering Mach waves. The eddy Mach waves are quadrupole and dipole radiations from the turbulent boundary layers developing in the nozzle and in the test section of a supersonic wind tunnel. The shivering Mach waves are generated from flaws in the nozzle contour

Presented at the 41st AIAA Fluid Dynamics Conference and Exhibit, Honolulu, Hawaii, June 26–30, 2011; received 15 July 2011; revision received 3 April 2012; accepted for publication 3 April 2012.

*Ph.D. Candidate, Aeronautics and Aerospace Department, Chaussée de Waterloo 72; currently Delft University of Technology, Department of Aerospace Engineering, Kluyverweg 2, Delft 2629, The Netherlands; masutti@vki.ac.be. Student Member AIAA.

†Diploma Course Student 2009-2010, Aeronautics and Aerospace Department, Chaussée de Waterloo 72; espinosa82@alice.it.

‡Associate Professor, Aeronautics and Aerospace Department, Chaussée de Waterloo 72; chazot@vki.ac.be. Member AIAA.

§Honorary Professor, Aeronautics and Aerospace Department, Chaussée de Waterloo 72; carbonaro@vki.ac.be.

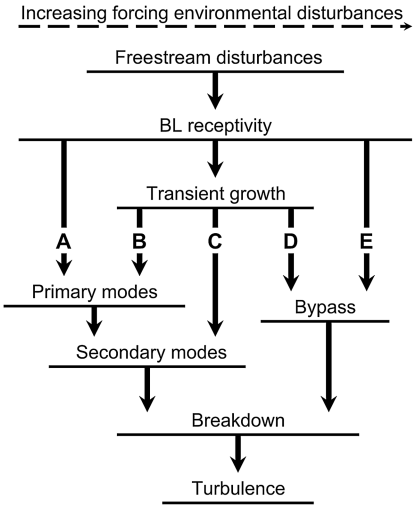

Fig. 1 Paths to transition (from Morkovin et al. [1]).

and they fluctuate in position when turbulence passes over them (Fig. 2). Eddy Mach wave radiation finds its theoretical basis in an extension of the Lighthill analogy (for the aeroacoustic production of sound) to a supersonic field. This extension was carried out by Phillips [8] and by Ffowcs-Williams and Maidanik [9]. At supersonic speeds, indeed, the relative velocity of quadrupole sources, responsible for sound generation according to Lighthill, is greater than the speed of sound. In this way, a mutual cancellation of waves cannot take place along the Mach wave direction, the dominant direction along which a monopole-type sound radiation results. Shivering Mach waves are described in more detail in Morkovin [10] and result in lower frequency fluctuations than the eddy Mach wave fluctuations.

These considerations were experimentally confirmed by Laufer [11], who showed that the disturbance field in the Jet Propulsion Laboratory Mach 5 wind tunnel, was dominated by sound waves, having an orientation slightly different from the Mach angle. Moreover, he showed that this sound pressure field was radiated by the turbulent boundary layers of the nozzle walls. These results can be generalized for all the supersonic and hypersonic wind tunnels, and constitute the starting point of the following analyses.

The knowledge of the physical origin of the disturbances can give way to some engineering solutions. This is the case of the so-called quiet wind tunnels [7]. The objective of these wind tunnels is to produce a low noise flow in the test section. Because the disturbances essentially originate in the turbulent boundary layer, most of these wind tunnels operate with boundary-layer suction in the throat, maintaining a laminar boundary layer along the nozzle walls and therefore reducing the disturbance level. This allows reproduction of ground test flow conditions much closer to flight, leading to transition studies in a low-noise environment, thus improving observation of the transition process itself.

In the framework of transition studies and the need for high-fidelity measurements in the boundary layer, a characterization of the freestream disturbance environment has been performed in the H3 Hypersonic Wind Tunnel of the von Kármán Institute (VKI) for Fluid Dynamics.

II. Experimental Setup

A. VKI H3 Mach 6 Hypersonic Wind Tunnel

The VKI H3 test facility is a blowdown to vacuum-type wind tunnel (Fig. 3). It can provide a uniform axisymmetric jet with a diameter of 12 cm at Mach 6. Dehumidified air is supplied from a 40 bar reservoir, which can provide stagnation pressures ranging from 6 to 35 bars. Air is heated to a total temperature of 500 K to avoid condensation in the test section. The Reynolds number of the flow can be varied between 3×10^6 and 30×10^6 m^{-1}. The wind tunnel is provided with a model injection mechanism to avoid blockage and also to avoid excessive heating of the model itself during startup. The test chamber is vacuumed before the test using a supersonic ejector. The wind-tunnel model is injected once the Mach 6 freejet is fully established.

B. Dual Hot-Wire Anemometry Setup

As extensively reported in the literature [12–17], a hot wire in supersonic/hypersonic flow is sensitive to two flow variables: mass flux ρu and total temperature T_0. To separate the contribution of these two variables in the hot-wire output, a simple probe containing a single wire is not sufficient:[¶] A special setup is necessary. Based on the work of Walker et al. [13] for hot-wire measurements, a dual hot-wire probe has been chosen for the present characterization. A picture of the probe is shown in Fig. 4. In the dual hot-wire anemometry technique, two hot-wire probes are connected to two separated constant temperature anemometry (CTA) electronic units. The two hot wires, 9-μm-diam tungsten wires with a 6.7% (refers to the thickness of the platinum coating with respect to the wire's diameter) platinum coating, are heated at different overheat ratios. Due to the oxidation problems and considering that the freestream recovery temperature is higher than the ambient temperature usually employed to define the overheat ratio, it was not possible to set the overheat ratio to a value higher than 1.9. To have an appreciable difference between the two overheat ratios, the lower overheat was set to 1.2.

The calibration of the dual wire probe is essential for the hot-wire anemometry measurements. For low overheat ratios, Smith and Smits [14] suggest using the following relation between the hot-wire voltage, the mass flux, and the total temperature:

$$E^2 = C_1 T_0^{a+1} + C_2 T_0^{a} + C_3 T_0^{a-1} + (\rho u)^n (C_4 T_0^{a-nb+1} + C_5 T_0^{a-nb} + C_6 T_0^{a-nb-1}) \tag{1}$$

For the present problem, it is assumed that $a = b = 0.768$ and $n = 0.55$ (as suggested by Smith and Smits [14]). Once the calibration relation is chosen, the calibration procedure provides the coefficients $C_1, C_2, \ldots, C_6$, present in Eq. (1). The procedure is schematized in Fig. 5, involving tests with different stagnation pressures and stagnation temperatures.

The determination of the coefficients is carried out for each single wire using a least-squares solution. The calibration tests are performed in situ because it is very difficult to reproduce the extreme conditions encountered both for mass flux and total temperature during a test in the VKI H3 Wind Tunnel. Once the calibration coefficients are determined, it is possible to reconstruct the instantaneous mass flux and total temperature signals from the direct hot-wire outputs solving a nonlinear system of equations for each instant, that is, for each sample of a time series (chart in Fig. 6).

The dynamic response of each anemometer is assessed by determining its maximum frequency response by means of the usual square wave test, performed at ambient conditions, but reproducing the values for mass flux encountered during a test in the VKI H3 Wind Tunnel. This procedure indicates a frequency response up to 25 kHz for the system with overheat ratio 1.9 and of 10 kHz for the system with overheat ratio 1.2 (see Sec. III.A). It should be noted that to use a quasi-steady calibration in the hot-wires data reduction, the signal of the high overheat ratio wire (25 kHz) has been low-pass filtered to match the frequency response of the lower overheat ratio wire (10 kHz). More details are reported in Spinosa et al. [18].

C. Pitot Pressure Measurement Setup

Pitot pressure measurements are carried out by means of a classical pitot probe, incorporating a fast response pressure transducer, flush mounted on its upstream extremity. The transducer used is a Kulite XCE-093-50A (B screen) designed for harsh environments and a wide temperature range. The pressure-sensing principle is based on

[¶]The use of a single hot wire would be possible only if equipped with a dedicated CTA scanning system, see Kosinov and Repkov [16] and Weiss et al. [17].

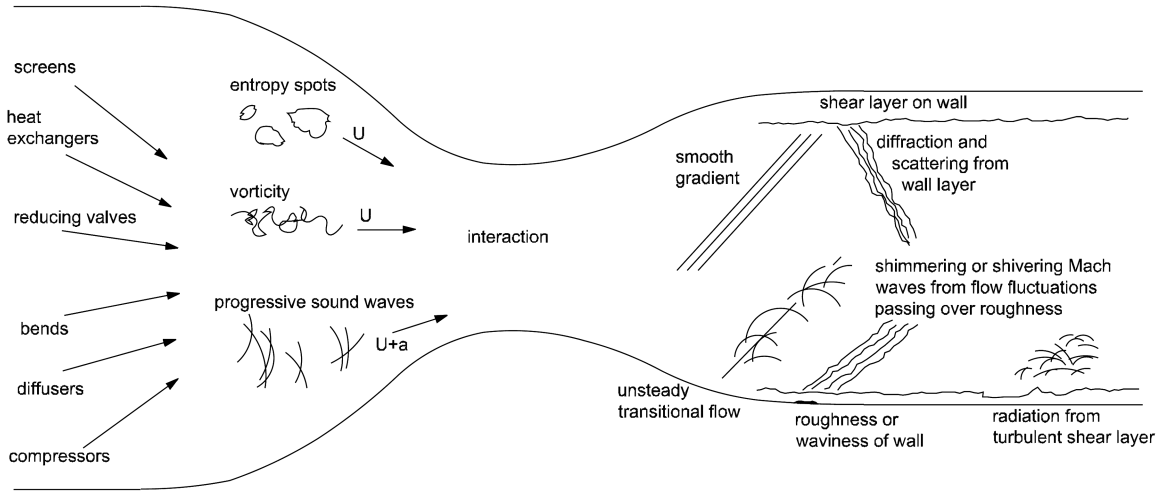

Fig. 2 Freestream disturbances in supersonic/hypersonic wind tunnels (from Schneider [7]).

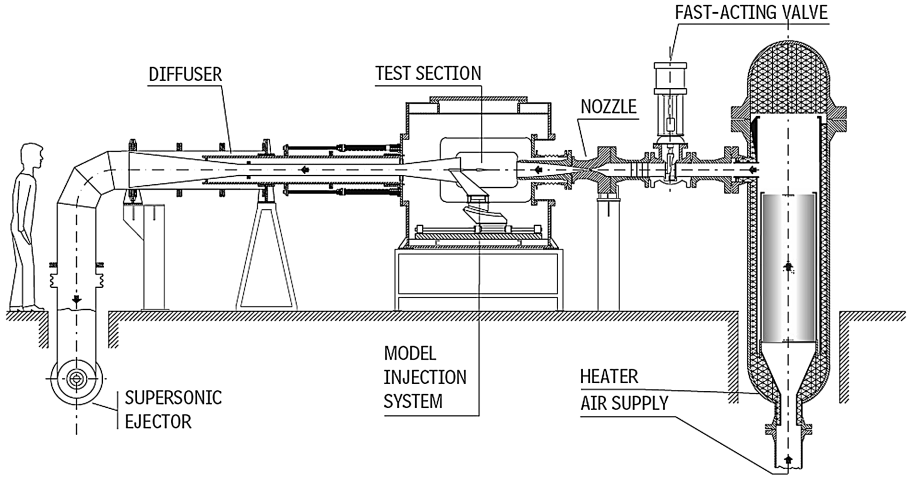

Fig. 3 VKI H3 Hypersonic Wind Tunnel.

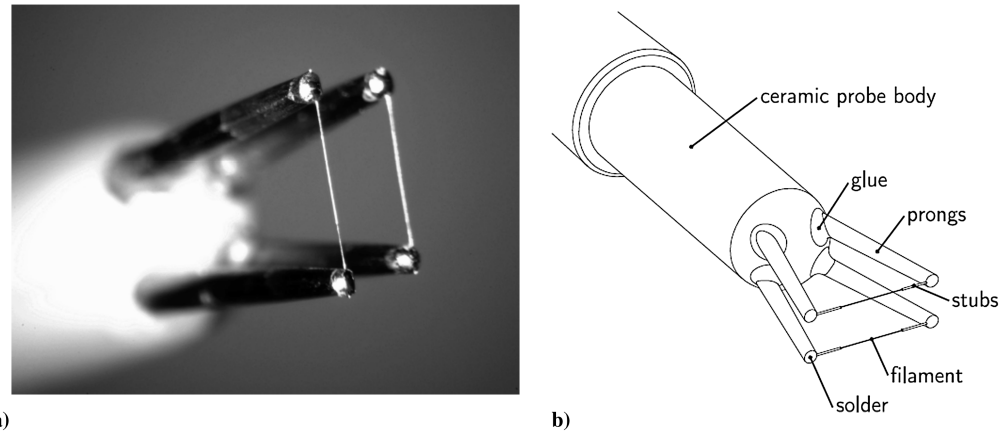

a) **b)**

Fig. 4 Double hot-wire probe: a) magnified picture of the wires, b) sketch of the double hot-wire probe.

an active four-arm strain gauge bridge diffused into a sculptured diaphragm for maximum sensitivity and wide-band frequency response up to 300 kHz, according to manufacturer's data. The pitot pressure probes are mounted in the rake support, also used for mounting the hot-wire probe (Fig. 7a). A schlieren of the pitot rake support (Fig. 7b) indicates that there is no interference of the shock wave existing in front of each pitot probe with the other probes of the rake, and in particular that there is no interference of the prongs and support of the hot-wire probe on the wire itself. During a test in the VKI H3 Wind Tunnel, the pitot probe undergoes an important aerothermodynamic heating, due to the stagnation point downstream of the normal shock [as can be seen in the computational fluid dynamics (CFD) computations shown in Fig. 8]. Because the miniature pressure transducer is directly facing the stagnation point, the temperature of its electronic chip changes during a test and can differ by about 50–100 K from the ambient temperature. Therefore, a static calibration of the transducer at ambient conditions is not valid, because it is well known that the transducer response strongly

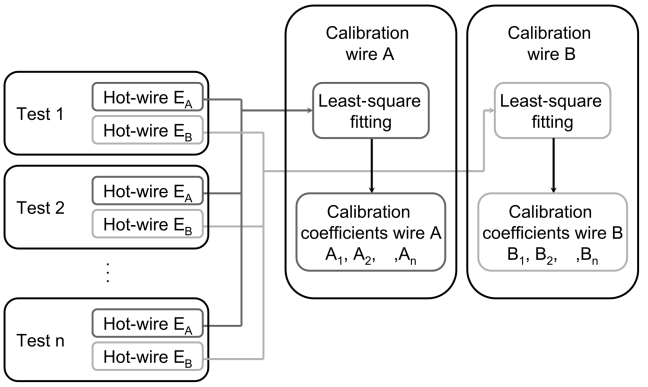

Fig. 5 Schematic of the hot-wire calibration procedure following the approach developed by Smith and Smits [14].

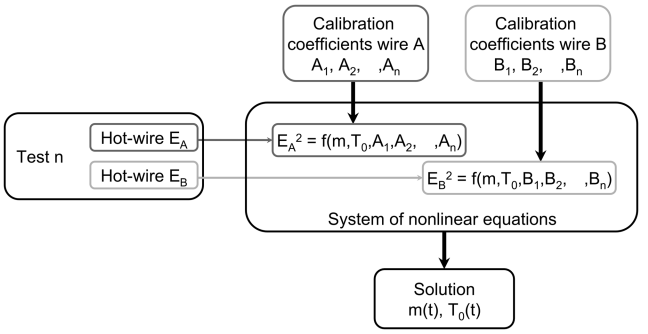

Fig. 6 Schematic of the hot-wire variable contribution separation following the approach developed by Smits et al. [12].

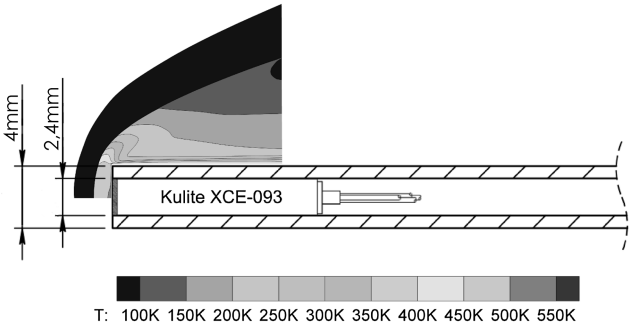

Fig. 8 CFD computation: static temperature of the fluid around the pitot probe for a generic test in the VKI H3 Wind Tunnel, $M = 6$, $T_0 = 500$ K, $p_0 = 21$ bar.

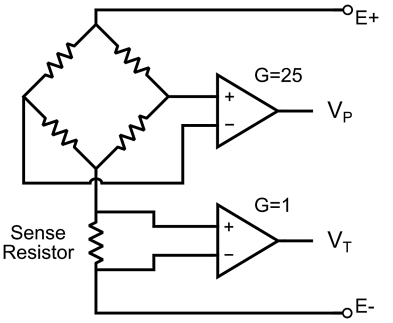

Fig. 9 Compensation circuit for piezoresistive pressure transducer [21].

depends on temperature. This dependence can be explained by the differing thermal coefficients of the resistive components on the Kulite diaphragm that lead to an unbalancing of the sensor bridge. (Moreover, temperature entails a nonlinear expansion of the transducer housing and the generation of other nonsymmetrical forces.) These effects result in an offset (zero drift) of the pressure transducer calibration law derived at ambient conditions, as well as a change of the sensitivity (scale or span drift), leading to a substantial under- or overestimation of the measured pressure. This change in sensitivity can be corrected and compensated by means of an adapted calibration technique, developed at Oxford University [19] and at VKI [20,21]. The technique is based on the assumption that the coefficients of the linear calibration law for a pressure transducer (slope and offset) also depend linearly on the temperature of the transducer chip; this assumption has also been verified by the Oxford University group [19]. Taking this into account, calibration tests can be performed during a transience with changes in both pressure and temperature. In the present work, the calibration tests are carried out in the transient phase before, during, and after the injection of the probe in the hypersonic jet. To monitor the variations of the chip temperature during this transience, an electronic circuit developed and built at the VKI is used. A conceptual schematic of the circuit is shown in Fig. 9. In this circuit, a resistor is placed in series with the Wheatstone bridge circuit. This particular design provides two outputs: The first one is the standard fast-response transducer voltage output, referred to as V_P; the second signal is proportional to the chip temperature and is referred to as V_T (this voltage signal is low-pass filtered because oscillations greater than 10 Hz are not expected to be significant due to the thermal capacity of the chip). Together with the fast-response pressure transducer probe flush mounted on a pitot probe, a second pitot probe, closely placed to the first one, has been used. This second pitot probe is simply connected by a tubing to an absolute pressure transducer located outside of the test section, which measures the mean value of the freestream pitot pressure P_{ref}. The latter is not affected by any temperature effect and can be used as an in situ reference for the pressure measured by the Kulite transducer P_{ku}. Assuming the coefficients of calibration to be linearly dependent on temperature, it is possible to search for a calibration relation for the fast-response pressure transducer of the form

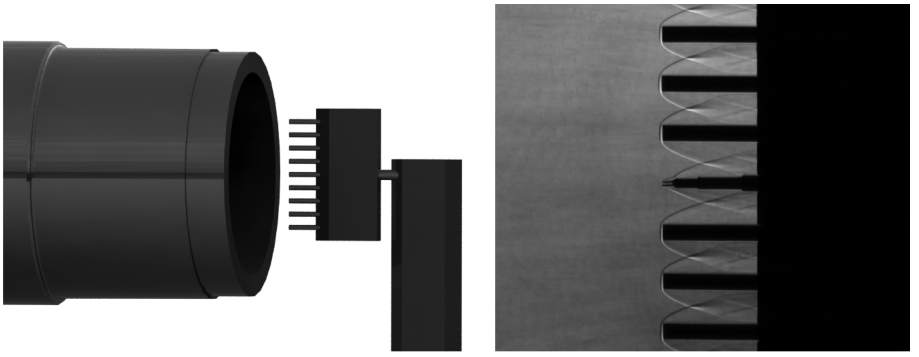

a) Pitot rake in front of the VKI H3 nozzle **b) Schlieren picture of the pitot rake**

Fig. 7 Rake support.

$$p_{\mathrm{ku}} = (C_1 V_T + C_2)V_P + (C_3 V_T + C_4) \tag{2}$$

The four coefficients $C_1, C_2, \ldots, C_4$ are computed by means of an optimization routine that represents a nondimensional form of the quadratic deviation of the fast-response pressure p_{ku} from the reference pressure P_{ref}. This is accomplished by minimizing the function

$$f = \sum^{N} \left[\frac{(p_{\mathrm{ku}} - p_{\mathrm{ref}})^2}{p_{\mathrm{ref}}^2} \right] \tag{3}$$

where N is the number of points for which the routine is applied (usually a subset of the original signal data points).

D. Combined Data Reduction and Modal Analysis

In the framework of this work, it was decided to apply a combined data reduction methodology, which can allow estimation of the level of fluctuation of all the flow quantities from those directly measurable using the previously described instrumentation. In a compressible flow, its turbulence description at a point is more complicated than in an incompressible flow. All the variables (e.g., pressure, velocity, temperature, etc.) show a certain degree of uncorrelated fluctuations, usually not predictable a priori [5]. The combined analysis, outlined in the literature [4,22–24], is valid under the following hypotheses: 1) perfect gas assumption; 2) small fluctuation for the dependent flow variables, $\frac{T'}{\bar{T}}, \frac{p'}{\bar{p}}, \frac{\rho'}{\bar{\rho}} \ll 1$; 3) small velocity fluctuations, $M_t = \frac{u'}{\bar{a}} \ll 1$; 4) measurements of wind-tunnel disturbances are not experiment dependent (unless in the case of wind-tunnel configuration changes), therefore, hot-wire or pitot pressure measurements can be performed separately without invalidating the statistical quantities; 5) measurements with hot wires and pitot pressure probe are not performed simultaneously, cross correlations are neglected; 6) in the case of pitot pressure measurements, pressure fluctuations are amplified passing through a strong shock wave [25], therefore, the postshock measured value is not underestimated if compared with the preshock one.

Under these hypotheses, the following equations are used:

$$m = \rho u \qquad p = \rho R T \qquad C_p T_0 = C_p T + u^2/2 \tag{4}$$

Introducing the Reynolds decomposition for all the variables involved and neglecting higher order terms, we obtain the following set of equations:

$$\frac{m'}{\bar{m}} = \frac{\rho'}{\bar{\rho}} + \frac{u'}{\bar{u}} \qquad \frac{p'}{\bar{p}} = \frac{\rho'}{\bar{\rho}} + \frac{T'}{\bar{T}} \qquad \frac{T_0'}{\bar{T}_0} = \alpha \frac{T'}{\bar{T}} + \beta \frac{u'}{\bar{u}} \tag{5}$$

where

$$\alpha = \left(1 + \frac{\gamma - 1}{2} M^2\right)^{-1} \qquad \beta = (\gamma - 1) M^2 \alpha \qquad M = \frac{\bar{u}}{\sqrt{\gamma R \bar{T}}} \tag{6}$$

The same results can be easily obtained by using the so-called logarithm derivative approach, used in Morkovin [26]: In this approach, the logarithmic derivative of each side of the equation is taken and the differential terms are interpreted as a small disturbance; results are analogous to Reynolds decomposition and elaboration. The system of Eq. (5) has six unknowns. If $\frac{m'}{\bar{m}}$ and $\frac{T_0'}{\bar{T}_0}$ are measured in the core of the hypersonic jet by means of the hot-wire anemometer and $\frac{p'}{\bar{p}}$ by a pressure probe, then it is possible to compute all the other fluctuation variables by solving the linear system Eq. (5) (three equations and three unknowns). To successfully apply the combined data reduction methodology, the pitot pressure measurements have to be treated to obtain the static pressure mean value and fluctuations. Because the flow impinging on the pitot probe is unsteady, application of the steady-flow equations to the instantaneous pitot pressure [27] in a quasi-steady approach is questionable, and it was invalidated by Stainback and Wagner [28]. To further verify this fact, the quasi-steady pitot-Rayleigh analysis [29,30] [Eq. (7)] was applied to obtain the fluctuations of static pressure from the fluctuations of pitot pressure, assuming that the pressure measured is insensitive to the angle of attack (within 20 deg) of the probe with respect to the flow up to Mach 6 [31]. The static pressure fluctuations can be estimated with the following quasi-steady pitot-Rayleigh equation:

$$p(t) = \frac{2 p_t(t)}{C_P \gamma M^2 + 2} \tag{7}$$

where

$$C_P = \frac{2}{\gamma M^2} \left[\frac{(\gamma + 1)^2 M^2}{4\gamma M^2 - 2(\gamma - 1)} \right]^{\gamma/(\gamma-1)} \left[\frac{1 - \gamma + 2\gamma M^2}{\gamma + 1} \right] - 1 \tag{8}$$

Applying Eq. (7) to every instantaneous value of a pitot pressure measurement, the instantaneous value of the static pressure is obtained. Fluctuations and mean value can then be computed from the static pressure time series. However, as said, in the early 1970s, Stainback and Wagner [28] invalidated the use of this quasi-steady equation for the pitot pressure flow analysis due to the overestimate of the computed static pressure fluctuations. The following unsteady approach [28] is therefore here used:

$$\frac{p_{\mathrm{rms}}}{\bar{p}} = \frac{\gamma}{2} \left(\frac{p_{t,\mathrm{rms}}}{\bar{p}_t} \right) \left[1 - \frac{4 n_x}{M} + 4 \left(\frac{n_x}{M} \right)^2 \right]^{-(1/2)} \tag{9}$$

where

$$n_x = \left(\frac{u_s - u_\infty}{u_\infty} \right)^{-1} M^{-1} \quad \text{and} \quad \frac{u_s}{u_\infty} = 0.6 \tag{10}$$

Figure 10 shows the static pressure fluctuations computed with the quasi-steady pitot-Rayleigh flow analysis [Eq. (7)] and the unsteady [Eq. (9)] approach by Stainback and Wagner [28]. The comparison confirms that the quasi-steady approach in general is overestimating by two times the correct static pressure fluctuations.

The solution of Eq. (9) provides the closure to the system of Eq. (5) for the combined analysis. The results are discussed in Sec. III.C. Once all flow fluctuations are derived from the data reduction, the modal analysis can be applied. The theory of the modal analysis has already been extensively presented by Kovasznay [5] and was further developed by Logan [22] and Smits and Dussauge [24]. A similar analysis was performed by Donaldson and Coulter [32], who reviewed 20 years of hot-wire and pitot pressure measurements in Arnold Engineering Development Center (AEDC) tunnels A and B, applying a modal analysis to evaluate the level and the source of disturbances in such wind tunnels. The purpose of the present investigation is therefore not to rediscuss the theory, but to apply it to an experimental case. The decomposition of the three modes is presented in Eq. (11), in which Θ is the entropy mode (temperature

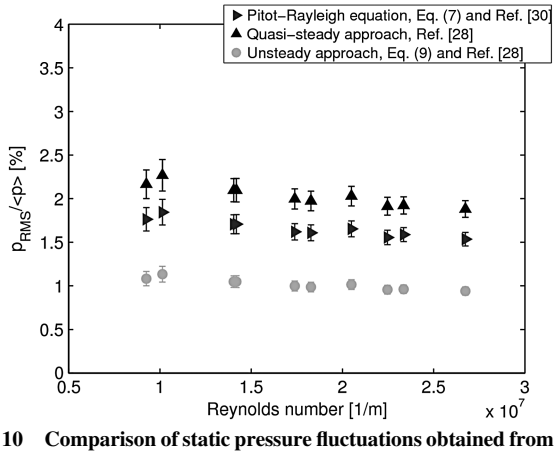

Fig. 10 Comparison of static pressure fluctuations obtained from pitot pressure measurements (Bowersox and Schetz [30], Stainback and Wagner [28]).

spottiness), ω is the vorticity mode, and σ is the sound-wave mode.

$$\Theta' = \frac{T'}{\bar{T}_0} - \frac{\gamma-1}{\gamma}\frac{\bar{T}}{\bar{T}_0}\frac{p'}{\bar{p}} \qquad \omega' = \frac{u'}{\bar{u}} + \frac{1}{\gamma M^2}\frac{p'}{\bar{p}} \qquad \sigma' = \left(1 - \frac{1}{M^2}\right)\frac{p'}{\gamma\bar{p}} \tag{11}$$

Equation (11), derived by the original theory of Kovasznay [5] and modified by Logan [22], take into account every single mode removing the contributions coming from the other two modes. The application of the modal analysis is straightforward and the results are discussed in Sec. III.C.

E. Uncertainty Quantification

The uncertainty analysis related to the experimental work has been performed using the Dakota code from the Sandia National Laboratories with Monte Carlo and Polynomial Chaos methods [33]. These two sampling techniques are useful, in cases like the present one, in which the system of nonlinear equations used for the calibration of the hot wires makes the propagation of error difficult to compute in the classical way using partial derivatives. Taking into account that the experimental error can be separated into a random error and a bias (systematic) error [34], several hypotheses have to be made:

1) The error given by the resolution of the acquisition system is negligible.

2) The random error can be identified as the standard deviation σ of the measured output voltage from a signal conditioner [35].

3) The bias error is the combination of the calibration error and the instrument error.

4) The error on each normalized fluctuation quantity is considered as the combination of the error on the mean value and the error on the nominal fluctuations.

5) All the uncertainties presented have been quantified with a confidence level of 95.45%.

Considering these hypotheses, the error on each derived quantity has been obtained cross correlating the results coming from Monte Carlo and Polynomial Chaos methods using an increasing number of sampling points. The results of these methods are summarized in Table 1, in which the errors on every normalized fluctuating variable are given. It can be noticed that the error on the mass flux is fairly high. This is presumably related to the high dispersion introduced by the nonlinear method used for the calibration of the hot wires. One has to remember that the errors estimated on the mean values are based on just one experiment for every Reynolds number. By increasing the number of experiments, the dispersion of the results and the relative error decrease with the square root of the number of tests performed [34]. To determine the sensitivity of the different measured values to the different derived quantities, the sensitivity coefficients have also been computed. Because the sensitivity due to the different parameters is not changing with the Reynolds number, an example of the sensitivity analysis is shown in Table 2 for the case at $Re/m = 9.89 \times 10^6$.

Table 2 shows how the velocity u, for example, is sensitive to the variation of mass flux m and in minor extent to the variation of total temperature T_0. The density ρ and the static temperature instead are mainly sensitive to the variation of the mass flux m only. Regarding the dependency of the modal variables, the entropy Θ is driven by the variation of mass flux m, whereas the vorticity ω is sensitive to the velocity u, that is, the mass flux m and the total temperature T_0. The sound-wave mode σ is highly linked to the static pressure p variations.

III. Experimental Results

Freestream disturbance measurements are carried out along the centerline of the VKI H3 Wind Tunnel. The fluctuations of the flow quantities are assumed to be uniform in the potential core of the test section jet. Although this hypotheses has not been proven yet for the VKI H3 Wind Tunnel, similar results are found in the literature, for example, in Wagner [36] for a hypersonic Mach 5 jet and, therefore, they are assumed valid for the present case as well. Tests are repeated for different unit Reynolds numbers, by varying the wind-tunnel supply pressure.

A. Hot-Wire Anemometer Measurements

Hot-wire measurements are conducted along the centerline of the hypersonic freejet at 10 mm downstream of the nozzle exit. As specified in Sec. II.B, tests are used both for the calibration and for the disturbance characterization: Data are acquired simultaneously by means of a National Instrument USB-6251 with 16-bit resolution at a sampling frequency of 500 kHz during an observation time of 0.5 s. The frequency response of the two hot wires is different, but in any case, no antialiasing filter was used because the frequency response of the wires is much lower than one-half of the sampling frequency used. In the present analysis, only results obtained by means of the calibration law proposed by Smith and Smits [14] for each wire are reported (see Sec. II.B). Other methods for the calibration of the hot-wire probe are reported in Spinosa et al. [18]. Statistical analyses are

Table 1 Uncertainty quantification on normalized fluctuations

Reynolds number, 10^6/m	Error m, %	Error T_0, %	Error p, %	Error u, %	Error ρ, %	Error T, %	Error Θ, %	Error ω, %	Error σ, %
9.89	78.16	6.12	7.60	17.85	43.53	38.36	40.87	18.30	7.06
10.13	71.55	5.84	7.95	13.52	41.10	33.83	37.23	13.98	7.36
10.53	66.43	5.67	N/D[a]	N/D	N/D	N/D	N/D	N/D	N/D
14.30	38.99	3.55	6.37	4.60	27.35	21.97	24.47	4.70	5.99
14.50	38.99	3.55	6.45	2.99	26.34	19.52	22.52	3.03	6.06
17.06	64.25	9.38	5.76	19.45	39.00	35.99	37.50	19.89	5.45
17.62	16.89	2.72	5.66	9.01	14.52	13.60	14.04	9.23	5.36
20.60	38.57	5.89	5.53	19.00	27.62	26.07	26.71	19.42	5.24
23.36	21.38	2.99	5.30	3.36	17.25	15.22	16.22	3.41	5.03
23.98	27.25	5.39	5.09	8.57	21.44	19.99	20.73	8.67	4.84
27.34	15.70	2.79	5.05	3.84	13.39	12.35	12.86	3.87	4.81

[a]N/D, no data.

Table 2 Sensitivity analysis on derived quantities ($Re/m = 9.89 \times 10^6$)

Input variable	Sensitivity coefficients					
	Velocity, u	Density, ρ	Static temperature, T	Entropy, Θ	Vorticity, ω	Sound wave, σ
Mass flux, m	0.799	0.995	0.981	0.990	0.803	0
Total temperature, T_0	0.187	0.003	0.007	0.006	0.189	0
Static pressure, p	0.014	0.002	0.011	0.004	0.008	1

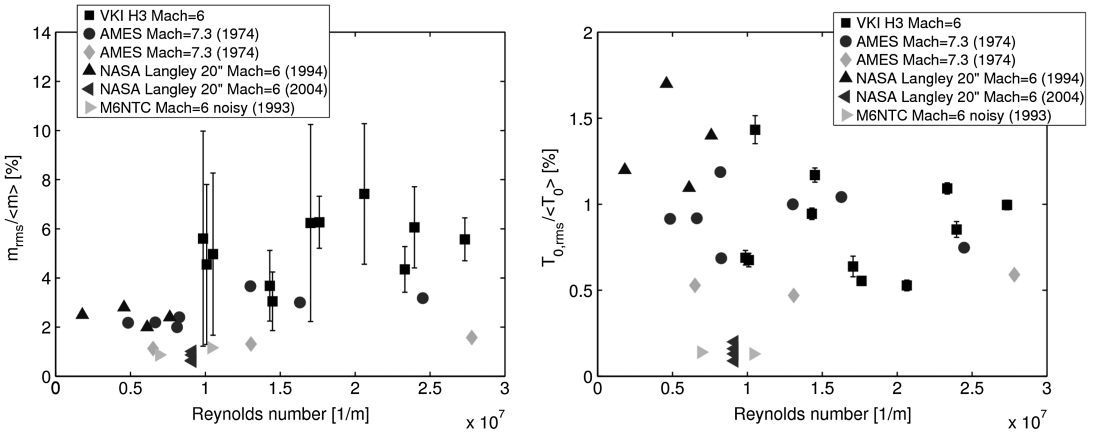

a) Normalized rms value of the mass flux **b) Normalized rms value of the total temperature**

Fig. 11 Normalized rms value of the mass flux and total temperature as function of the unit Reynolds number (present investigation and data replotted from Owen [23], Stainback and Kubendran [37], and Chokani et al. [38]).

carried out of the mass flux and total temperature signals to provide information about the intensity of the fluctuations of the two flow quantities. In Fig. 11, the normalized rms of the mass flux and total temperature fluctuations measured with the hot-wire probe are given as a function of the freestream unit Reynolds number. The values of the normalized mass flux rms are between 3 and 7%, whereas the values of the normalized total temperature rms are around 1%. It is also possible to see that the mass flux fluctuations and the total temperature fluctuations do not show a definite trend, and therefore do not have any dependency on the Reynolds number. Assuming that the sound waves are the source of all fluctuations in a Mach 6 hypersonic wind tunnel, the total temperature fluctuations should be around 3 and 4% of the mass flux fluctuations [37]. In their investigation conducted in the Langley 20 in. Mach 6 Wind Tunnel, Stainback and Kubendran [37] reported total temperature fluctuations on the order of half the mass flux fluctuations. They concluded that a part of the total temperature fluctuation could be related to the entropy spottiness due to the absence of a thermal equalizer system upstream of the wind tunnel. Similar results were also found in other hypersonic facilities [39]. The data shown in Fig. 11 indicate that the total temperature fluctuations in the VKI H3 Wind Tunnel are about 20% of the mass flux fluctuations. Therefore, a similar conclusion to the one of Stainback can be made, that is, part of such high total temperature fluctuations could be caused by entropy spottiness. Fig. 12 shows the power spectral density for the hot-wire output signals not yet filtered. The power spectral density is computed by means of the Welch Periodogram Method with intervals of 2^{16} points and an overlapping of 25%. The term "noise" refers to an acquisition carried out just before the test itself, without flow but with the hot-wire conditioner turned on: This acquisition gives information about the electronic and environmental noise sensed by the electronics. Immediate from the graph in Fig. 12 are the different frequency responses of the two hot-wire systems: In particular, the power spectral density of the low overheat ratio wire system (HW2) shows a flattening of the power spectral density (PSD) around 5 kHz, a lower than expected value from the square wave test. This consideration must be taken into account as another source of error in the disturbance measurements. In the low overheat case, the background noise is likely to disturb the frequency content of the signal in a more important way. In other words, the signal-to-noise ratio is lower for the low overheat ratio wire than for the high overheat ratio wire. In the spectra of Fig. 12, a peak is observed for the signal of the high overheat ratio wire (HW1) around 50 kHz. The nature of this peak, also reported by Mangalam et al. [40] and Stainback and Kubendran [37], is still unknown.

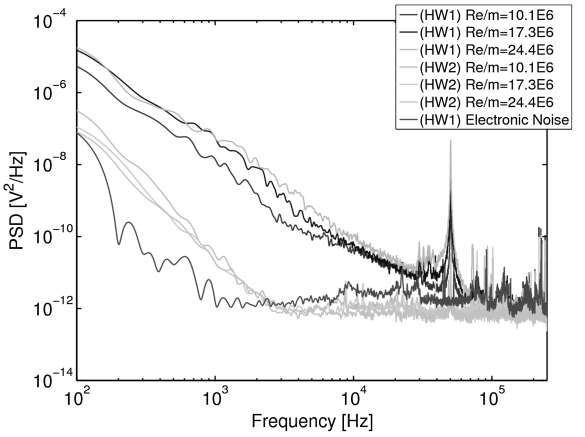

Fig. 12 Power spectral density for the double hot-wire at different Reynolds number.

B. Pitot Pressure Measurements

Pitot pressure measurements are carried out by means of the instrumentation described in Sec. II.C. For each test, two out of the nine probes of the rake are used; the pitot probe incorporating the Kulite pressure transducer is placed along the centerline of the nozzle. The streamwise distance between the probe tip and the nozzle exit is about 10 mm. The other pitot probe, connected to the reference pressure transducer, is located at a spanwise distance of 12 mm with respect to the centerline.** During each test, the two outputs are recorded by means of a National Instrument PXI-6133 with 14-bit resolution, sampled at 1 MHz during an observation time of 5 s. Because the natural frequency of the Kulite pressure transducer is much lower than half the sampling frequency, no antialiasing filter was used. In Fig. 13a, the normalized rms, indicated as NRMS is plotted against the unit Reynolds number of the flow, computed from the VKI H3 settling chamber measurements. NRMS values are around 1.7%. As it is possible to see, the NRMS values have an inverse linear dependency from the unit Reynolds number, which is coherent with the theory of the stabilizing effect of the increasing Reynolds number. Similar results were also obtained by Wagner [36] and Stainback et al. [28,43] for the NASA Langley Mach 5 Wind Tunnel, more recently by Lafferty and Norris [41] in the AEDC Hypervelocity Wind Tunnel and by Steen in the Boeing/AFOSR Mach-6 Quiet Tunnel (BAM6QT) [42]. In Fig. 13b, the pitot pressure fluctuations of the VKI H3 Wind Tunnel are compared with those measured by Stainback and Wagner in the Langley Mach 5 Wind Tunnel [28]. As can be seen, the level of pressure fluctuations, as well as the decreasing trend of their amplitude caused by the

**As mentioned before, it is possible to assume that the mean values and the fluctuating values of the flow quantities do not vary in the potential core of the jet itself [36]; consequently, the two measurements should provide equivalent results.

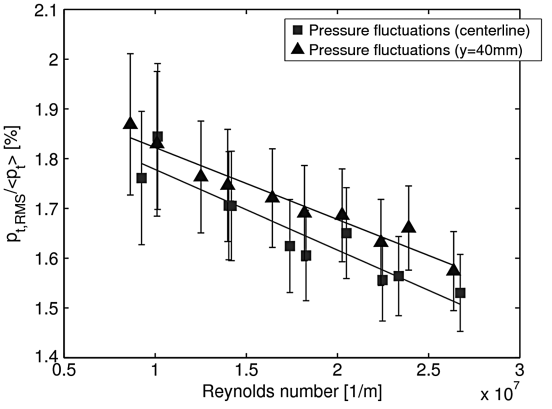

a) Unit Reynolds number dependency of pitot pressure fluctuations

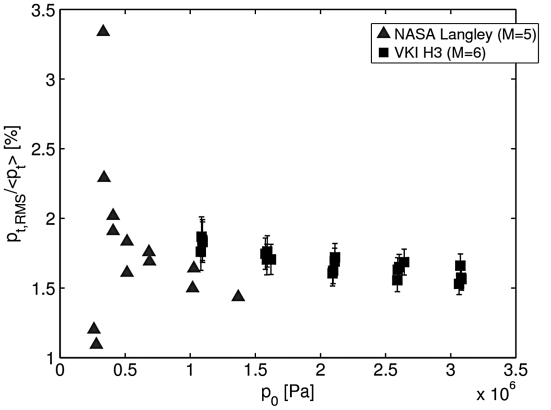

b) Comparison of pitot pressure fluctuations with results from Stainback and Wagner [28]

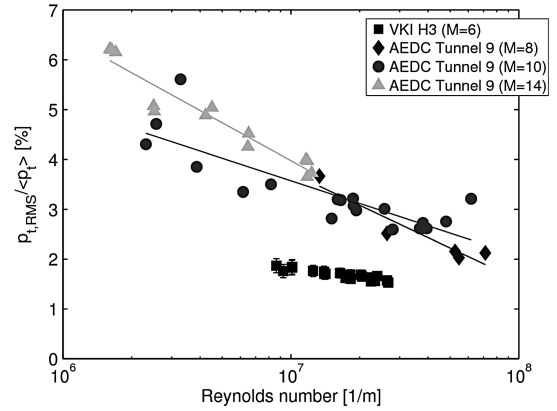

c) Comparison of pitot pressure fluctuations with results from Lafferty and Norris [41]

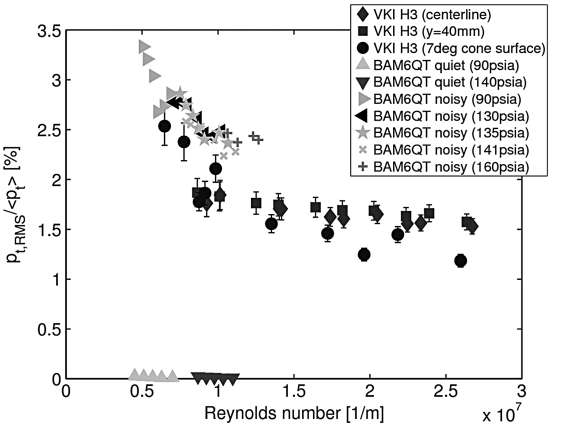

d) Comparison of pitot pressure fluctuations with results from Steen [42]

Fig. 13 Pressure fluctuations comparison.

Reynolds number stabilizing effect are very well matching. A similar comparison can be done between the VKI H3 and the AEDC Hypervelocity Wind Tunnel in Fig. 13c, where again the level of pressure fluctuations are comparable and, in particular, are lower by about 60% with respect to the fluctuations obtained in the AEDC tunnel at higher Mach numbers. Comparing the VKI H3 with the BAM6QT (Fig. 13d) for a very similar Mach number of 6, the pressure fluctuations in the freestream of the VKI H3, as well as on a 7 deg half-cone, match fairly well with the pressure fluctuations measured in the BAM6QT under noisy flow conditions. The situation changes drastically if the VKI H3 pressure fluctuations are compared with the BAM6QT under quiet flow conditions where the pressure fluctuations drop to about 0.015%. Stainback and Wagner [28] stress the point that the disturbance field of a hypersonic wind tunnel is mainly dominated by the sound radiated from the boundary layer developing on the nozzle walls. Consequently, it has a preferred orientation, which is very close to the characteristic line inclined at the Mach angle. Therefore, the probe in the flowfield is sensitive mostly to the disturbances that originate from the turbulent boundary layer on the nozzle walls. In Fig. 14a, the power spectral density of

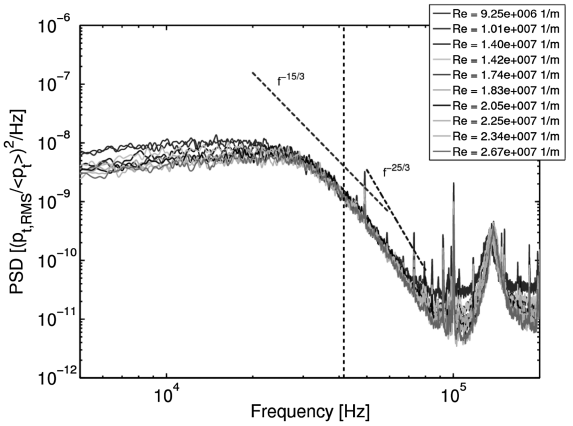

a) Power spectral density of normalized pitot pressure fluctuation

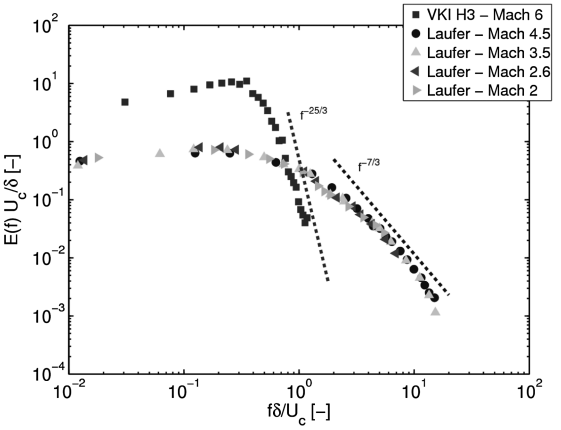

b) Energy spectrum of pressure fluctuation for various supersonic Mach numbers (from Laufer [44])

Fig. 14 Pitot pressure fluctuations power spectral densities.

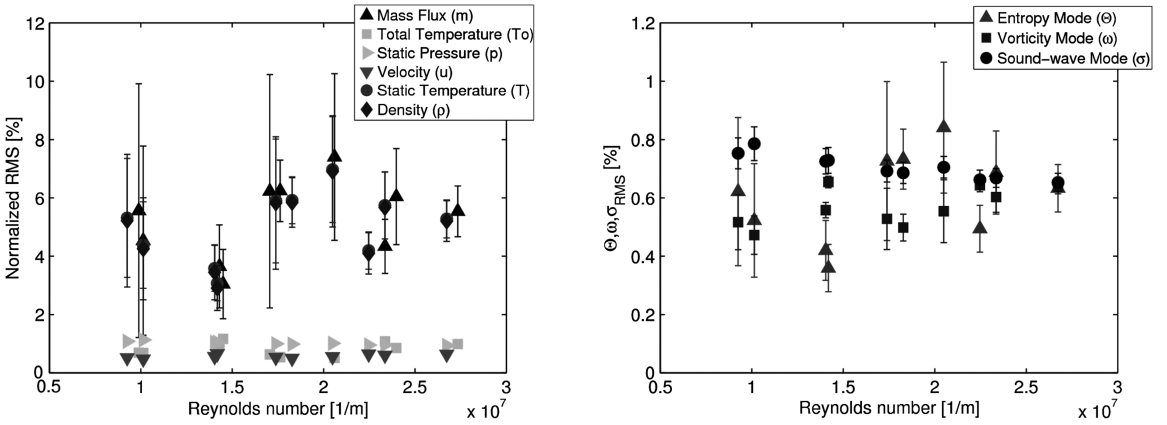

a) Results from the combined data reduction for VKI H3 Wind Tunnel

b) Results for the VKI H3 Wind Tunnel from application of Kovasznay modal analysis [6], fluctuations of the modes

Fig. 15 Disturbance level in the VKI H3.

the signals is plotted against the frequency in a double logarithmic scale. The PSD is computed using the Welch Modified Periodogram Method, with a number of points per interval equal to $2^{16} = 65,536$ and with an overlapping of 25% in each interval. Peaks in the PSD are clearly present around a frequency of about 135 kHz. These peaks are possibly related to the Helmholtz resonance of the cavity between the external screen, which shields the transducer, and the actual sensor membrane. Indeed, some preliminary calculations have shown that the order of magnitude of the resonance frequency is the same as the frequency of these peaks. However, the Helmholtz frequency depends strongly on the local speed of sound and therefore on the local temperature of the cavity. This temperature depends on the viscous effects, and this may be a reason why the small shift in frequency of the peaks is directly related to the Reynolds number. To correctly analyze the PSD in Fig. 14a, we must also take into account the transducer size effect. The pressure transducer output is proportional to the integrated pressure force on its active area, effectively averaging out fluctuations with characteristic wave length smaller or comparable to the probe tip size. A simplified hypotheses can be applied, yielding a firsthand estimation of the probe high-frequency response. Supposing an active probe diameter of about 1.8 mm, which yields a wavenumber [defining the wavenumber as $k = 2\pi f/v_p$, where v_p is equal to the freestream velocity ($\approx$940 m/s)] of about 560 m^{-1}, assuming that the Nyquist theorem is applicable, the frequency (wavenumber) response of the probe is 42 kHz (280 m^{-1}).

For every unit Reynolds case, the PSD shows an almost flat response until approximately 22–30 kHz, after which it starts to decrease, as expected in a turbulent freestream. Considering the high-frequency response limit of the probe (vertical black line in Fig. 14a), the energy decay for frequencies between 30–45 kHz follows a trend around $f^{-15/3}$, whereas for frequencies between 45–90 kHz, the energy decay is steeper (around $f^{-25/3}$). In any case, the energy decay $f^{-15/3}$ of the pressure fluctuations in the VKI H3 Wind Tunnel is above Kolmogorov's $k^{-7/3}$ law for pressure fluctuations decay (see George et al. [45]). The results obtained by Laufer [44] after a suitable normalization and reported in Fig. 14b indicate a decay of the energy spectrum for pressure fluctuations in supersonic flows, which follows a trend of $f^{-7/3}$. Laufer further proved that such a decay is typical of a noisy supersonic wind tunnel, which is dominated by eddy Mach waves. Comparing the $f^{-15/3}$ decay of the energy spectrum of the pressure fluctuations in the VKI H3 (considering the spatial resolution of the pitot probe) with the $f^{-7/3}$ decay measured by Laufer [44], the VKI H3 shows a steeper spectrum, which could indicate a different influence of the eddy Mach waves on the freestream. Nevertheless, the VKI H3 Wind Tunnel is still a conventional noisy wind tunnel affected by disturbances with a relatively wide range of frequencies (up to 30 kHz); this broadband frequency content is typical of the acoustic disturbances in the flow and provide a verification of their dominant sound-wave nature (see modal analysis and Fig. 15b).

C. Modal Analysis

The results from the combined data reduction process are shown in Fig. 15a. Fluctuations of the static temperature and density are closely related to the fluctuations of mass flux (between 3 and 7%), whereas velocity fluctuations are stable around 0.6% for varying unit Reynolds number. Indeed, if we consider Eq. (5) and that $\frac{u'}{\bar{u}} < 1$, then $\frac{m'}{\bar{m}} \approx \frac{\rho'}{\bar{\rho}}$, for the same reason, considering the law of the perfect gas, the density is a function of the static pressure and the static temperature; therefore, if $\frac{p'}{\bar{p}} \approx 1$ then $\frac{m'}{\bar{m}} \approx \frac{\rho'}{\bar{\rho}} \approx \frac{T'}{\bar{T}}$. Summarizing, mass flux fluctuations, total temperature fluctuations, and pressure fluctuations in the freestream are, respectively, on the order of 5.2, 0.8, and 1%; whereas derived quantities such as density fluctuations, static temperature fluctuations, and velocity fluctuations are on the order of 4.9, 5.2, and 0.6%. The origin of the disturbances in the VKI H3 can be identified from the results of the Kovasznay modal analysis (Fig. 15b), from which it appears that the three modes are uncorrelated, thus substantiating the concept that the disturbances that contribute to the freestream noise are generated by different sources [5]. The sound-wave mode (around 0.71%) appears to be predominant in the VKI H3 Wind Tunnel for the whole Reynolds number range, whereas the entropy and vorticity modes are both around 0.6%. All the three modes are contributing in the flow fluctuations and the sound wave in a major extent. This latter consideration confirms the predominance of freestream disturbances propagating from the turbulent boundary layer on the nozzle walls (see Morkovin [10] and Laufer [11,44]).

IV. Conclusions

An experimental characterization of the freestream jet of the von Kármán Institute (VKI) H3 Wind Tunnel was carried out by means of classical intrusive techniques: For this purpose, mass flux, total temperature, and pressure fluctuations were measured using a double hot-wire probe and a fast-response pitot probe in combination with suitable data reduction techniques.

Mass flux fluctuations show larger values with respect to the total temperature fluctuations, respectively, around 5.2 and 0.8%. As far as the total temperature fluctuations are concerned, it is possible to notice that their values are smaller than the mass flux fluctuations, but they are not as small as they would be if the radiated sound was the only dominant characteristic of the disturbance field. This consideration, together with the fact that the VKI H3 Wind Tunnel does not have any thermal equalizing system, leads one to think that the entropy spottiness mode can also have an important role in the freestream disturbance of the freestream jet.

Mass flux fluctuations show a bigger amplitude compared with other hypersonic facilities in the same Mach number range and the reason could be associated with entropy fluctuations in the flow. Pitot measurements have shown the classical trend expected for the supersonic/hypersonic wind-tunnel facilities. Because the disturbance field is dominated by sound waves radiated by the turbulent boundary layers on the nozzle wall, this sound has a preferred orientation, which is close to the Mach waves direction. The normalized pitot pressure fluctuations are around 1.7% and show a decreasing trend with the increasing unit Reynolds number (stabilizing effect of the Reynolds number). Regarding the energy content in the spectra, a peak due to Helmholtz resonance is present around 135 kHz, at a frequency slightly increasing with the increasing Reynolds number. After an almost flat energy content up to 30 kHz, the energy starts decaying with a slope close to $f^{-15/3}$, above Kolmogorov's $k^{-7/3}$ law for pressure decay. This decay becomes steeper ($f^{-25/3}$) at frequencies above 42 kHz due to the transducer size, which prevents resolving higher frequencies. This energy decay is a sign of a slightly turbulent flow or a laminar flow that is strongly affected by nozzle wall-generated noise (eddy Mach waves). Moreover, the wide-frequency content up to 30 kHz in the power spectral density is an indirect confirmation of the predominance of the sound disturbance mode in the flow, which is characterized by high frequencies.

The combined data reduction brings more information regarding the fluctuation of the fluid dynamic variables in the jet core. Fluctuations of the static temperature and density are between 3 and 7%, whereas velocity fluctuations are on the order of 0.6%. The latter is a demonstration of the turbulent nature of the freestream flow. Summarizing, the VKI H3 Wind Tunnel is a conventional noisy wind tunnel with a low turbulence intensity, but the freestream is dominated by sound-wave disturbances (eddy Mach waves) with slightly larger amplitudes than entropy and vorticity fluctuations.

References

[1] Morkovin, M., Reshotko, E., and Herbert, T., "Transition in Open Flow Systems—A Reassessment," *Bulletin of the American Physical Society*, Vol. 39, No. 9, 1994, p. 1882.

[2] Saric, W., White, E., and Reed, H., "Boundary-Layer Receptivity to Freestream Disturbances and Its Role in Transition," *30th AIAA Fluid Dynamics Conference*, AIAA Paper 1999-3788, 1999.

[3] Pate, S., "Effect on Wind Tunnel Disturbances on Boundary Layer Transition, with Emphasis on Radiated Noise: A Review," AIAA Paper 80-0431, March 1980.

[4] Owen, F. K., and Owen, A. K., "Measurement and Assessment of Wind Tunnel Flow Quality," *Progress in Aerospace Sciences*, Vol. 44, No. 5, 2008, pp. 315–348. doi:10.1016/j.paerosci.2008.04.002

[5] Kovasznay, L. S. G., "Turbulence in Supersonic Flow," *Journal of Aeronautical Sciences*, Vol. 20, No. 10, 1953, pp. 657–674.

[6] Morkovin, M., "On Transition Experiments at Moderate Supersonic Speeds," *Journal of the Aeronautical Sciences*, Vol. 24, No. 7, 1957, pp. 480–486.

[7] Schneider, S. P., "Development of Hypersonic Quiet Tunnels," *Journal of Spacecraft and Rockets*, Vol. 45, No. 4, Aug. 2008, pp. 641–664. doi:10.2514/1.34489

[8] Phillips, O., "On the Generation of Sound by Supersonic Turbulent Shear Layers," *Journal of Fluid Mechanics*, Vol. 9, No. 1, 1960, pp. 1–28. doi:10.1017/S0022112060000888

[9] Ffowcs-Williams, J. E., and Maidanik, G., "The Mach Wave Field Radiated by Supersonic Turbulent Shear Flows," *Journal of Fluid Mechanics*, Vol. 21, No. 4, 1965, pp. 641–657. doi:10.1017/S0022112065000393

[10] Morkovin, M., "On Supersonic Wind Tunnels with Low Free-Stream Disturbances," *Journal of Applied Mechanics*, Vol. 26, No. 3, 1959, pp. 319–323.

[11] Laufer, J., "Aerodynamic Noise in Supersonic Wind Tunnels," *Journal of the Aerospace Sciences*, Vol. 28, No. 9, Sept. 1961, pp. 685–692.

[12] Smits, A. J., Hayakawa, K., and Muck, K. C., "Constant Temperature Hot-Wire Anemometer Practice in Supersonic Flows," *Experiments in Fluids*, Vol. 1, No. 2, 1983, pp. 83–92. doi: 10.1007/BF00266316

[13] Walker, D., Ng, W., and Walker, N., "Experimental Comparison of Two Hot Wire Techniques in Supersonic Flow," *AIAA Journal*, Vol. 27, No. 8, Aug. 1989, pp. 1074–1080. doi:10.2514/3.10223; also AIAA Paper 88-0422.

[14] Smith, D. R., and Smits, A. J., "Simultaneous Measurement of Velocity and Temperature Fluctuations in the Boundary Layer of a Supersonic Flow," *Experimental Thermal and Fluid Science*, Vol. 7, No. 3, 1993, pp. 221–229. doi:10.1016/0894-1777(93)90005-4

[15] Spina, E., and McGinley, C. B., "Constant-Temperature Anemometry in Hypersonic Flow: Critical Issues and Sample Results," *Experiments in Fluids*, Vol. 17, No. 6, 1994, pp. 365–374. doi:10.1007/BF01877036

[16] Kosinov, A., and Repkov, V., "Design and Application of CTA in Supersonic Flow," *International Conferences on Methods of Aerophysical Research*, Novosibirsk, Russia, 1998.

[17] Weiss, J., Knauss, H., and Wagner, S., "Experimental Determination of the Freestream Disturbance Field in a Short-Duration Supersonic Wind Tunnel," *Experiments in Fluids*, Vol. 35, No. 4, 2003, pp. 291–302. doi:10.1007/s00348-003-0623-z

[18] Spinosa, E., Masutti, D., and Chazot, O., "Experimental Characterization of the Disturbance Level of the VKI H3 Wind Tunnel," von Kármán Inst., TR PR-2010-32, June 2010.

[19] Ainsworth, R., "Recent Development in Fast Response Aerodynamic Technology," *Measurement Techniques II*, Vol. 1, LS-von Karman Institute for Fluid Dynamics, 1995.

[20] Dènos, R., "Influence of Temperature Transients and Centrifugal Force on Fast Response Pressure Transducers," *Experiments in Fluids*, Vol. 33, No. 2, 2002, pp. 256–264. doi: 10.1007/s00348-002-0408-9

[21] Arts, T., Boerrigter, H.-L., Buchlin, J.-M., Carbonaro, M., and Degrez, G., *Introduction to Measurement Techniques in Fluid Dynamics*, von Kármán Institute for Fluid Dynamics, Rhode-St-Genese, Belgium, 2001.

[22] Logan, P., "Modal Analysis of Hot-Wire Measurements in Supersonic Turbulence," *26th AIAA Aerospace Sciences Meeting*, AIAA Paper 1988-423, Jan. 1988.

[23] Owen, F., "Transition and Turbulence Measurements in Hypersonic Flows," *Second AIAA International Aerospace Planes Conference*, AIAA Paper 90-5231, Jan. 1988.

[24] Smits, A. J., and Dussauge, J.-P., *Turbulent Shear Layers in Supersonic Flow*, American Inst. of Physics, Melville, NY, 1996.

[25] Mahesh, K., Lee, S., Lele, S. K., and Moin, P., "The Interaction on an Isotropic Field of Acoustic Waves with a Shock Wave," *Journal of Fluid Mechanics*, Vol. 300, 1995, pp. 383–407. doi:10.1017/S0022112095003739

[26] Morkovin, M. V., "Fluctuations and Hot-Wire Anemometry in Compressible Flows," AGARDograph, TR 24, 1956.

[27] Harvey, W. D., Bushnell, D. M., and Beckwith, I. E., "Fluctuating Properties of Turbulent Boundary Layers for Mach Numbers Up To 9," NASA, TR TN D-5496, Oct. 1969.

[28] Stainback, P. C., and Wagner, R. D., "A Comparison of Disturbance Levels Measured in Hypersonic Tunnels Using Hot- Wires Anemometer and a Pitot Pressure Probe," *Seventh AIAA Aerodynamic Testing Conference*, AIAA Paper 72-1003, Palo Alto, Sept. 1972.

[29] Anderson, J. D., *Hypersonic and High Temperature Gas Dynamics*, AIAA, Reston, VA, Aug. 2000.

[30] Bowersox, R. D. W., and Schetz, J. A., "Measurements of Compressible Turbulent Flow Structure in a Supersonic Mixing Layer," *AIAA Journal*, Vol. 33, No. 11, Nov. 1995, pp. 2101–2106. doi:10.2514/3.12953

[31] Norris, J. D., "Calibration of Conical Pressure Probes for Determination of Local Flow Conditions at Mach Numbers from 3 to 6," NASA, TR TN D-3076, 1965.

[32] Donaldson, J., and Coulter, S., "A Review of Free-Stream Flow Fluctuation and Steady-State Flow Quality Measurements in the AEDC/VKF Supersonic Tunnel A and Hypersonic Tunnel B," *Sixth AIAA International Space Planes and Hypersonic Systems and Technologies Conference*, AIAA Paper 95-6137, April 1995.

[33] Adams, B. M., Bohnhoff, W. J., Dalbey, K. R., Eddy, J. P., Eldred, M. S., Gay, D. M., Haskell, K., Hough, P. D., and Swiler, L. P., *DAKOTA, A Multilevel Parallel Object- Oriented Framework for Design Optimization, Parameter Estimation, Uncertainty Quantification, and Sensitivity Analysis: Ver. 5.0 User's Manual*, Sandia Technical Rept. SAND2010-2183, Dec. 2009.

[34] Oppenheim, A. V., and Willsky, A. S., *Signals and Systems*, Prentice–Hall, Upper Saddle River, NJ, 1997.

[35] Dènos, R., and Paniagua, G., "Fundaments of Data Acquisition and Processing," *Course Note 171*, von Kármán Inst. for Fluid Dynamics, Rhode-St-Genese, Belgium, Oct. 2005 (revised edition).

[36] Wagner, R., "Mean Flow and Turbulence Measurements in a Mach 5 Free Shear Layer," NASA Langley Research Center, TR TN D-7366, 1973.

[37] Stainback, P., and Kubendran, L., "The Measurement of Disturbance Levels in the Langley Research Center 20-Inch Mach 6 Tunnel," NASA, TR CR-4571, 1994.

[38] Chokani, N., Shiplyuk, A. N., Sidorenko, A. A., and McGinley, C. B., "Comparison Between a Hybrid Constant-Current Anemometer and Constant-Voltage Anemometer in Hypersonic Flow," *34th AIAA Fluid Dynamics Conference and Exhibit, Portland*, AIAA Paper 2004-2248, June 2004.

[39] Stainback, P. C., Wagner, R. D., Owen, F. K., and Horstman, C. C., "Experimental Studies of Hypersonic Boundary-Layer Transition and Effects of Wind-Tunnel Disturbance," NASA Langley Research Center, TR TN D-7453, March 1974.

[40] Mangalam, S., Sarma, G., Kuppa, S., and Kubendran, L., "A New Approach to High-speed Flow Measurements Using Constant Voltage Anemometry," *17th AIAA Aerospace Ground Testing Conference*, AIAA Paper 92-3957, June 1992.

[41] Lafferty, J. F., and Norris, J. D., "Measurements of Fluctuating Pitot Pressure, Tunnel Noise, in the AEDC Hypervelocity Wind Tunnel No. 9," *U.S. Air Force T&E Days*, AIAA Paper 2007-1678, 2007.

[42] Steen, L., "Characterization and Development of Nozzles for a Hypersonic Quiet Wind Tunnel," M.S. Thesis, Purdue Univ., West Lafayette, IN, Dec. 2010.

[43] Stainback, P., Anders, J., Keefe, L., and Beckwith, I., "Sound and Fluctuating Disturbance Measurements in the Settling Chamber and Test Section of a Small, Mach 5 Wind Tunnel," *ICIASF'75 (Sixth International Congress on Instrumentation in Aerospace Simulation Facilities)*, Institute of Electrical and Electronics Engineers, Inc., New York, Sept. 1975, pp. 329–340.

[44] Laufer, J., "Sound Radiation from a Turbulent Boundary Layer," *In Mécanique de la Turbulence, Centre National de la Recherche Scientifique (CNRS)*, No. 108, Paris, 1962, pp. 381–393.

[45] George, W. K., Beuther, P. D., and Arndt, R. E. A., "Pressure Spectra in Turbulent Free Shear Flows," *Journal of Fluid Mechanics*, Vol. 148, 1984, pp. 155–191.
doi:10.1017/S0022112084002299

M. Choudhari
Associate Editor